Influence of limiting the projection region on coarse Large Eddy Simulation-Actuator Line Model simulations

M Draper[1], B López[1], A Guggeri[1], F Campagnolo [2], G Usera[1]

[1]Grupo de Mecánica de los Fluidos Computacional, Instituto de Mecánica de los Fluidos e Ingeniería Ambiental, Facultad de Ingeniería, Universidad de la República.
[2]Wind Energy Institute, Technische Universität München, Boltzmannstraße 15, D-85748 Garching bei München, Germany.

E-mail: mdraper@fing.edu.uy

Abstract. Wind energy has developed worldwide, becoming a mature technology. Nevertheless, major advances regarding wind turbine aerodynamics and control as well as wind farm control and its integration in the power grid are being foreseen in the near future. To accomplish that, different simulation tools have emerged. The Actuator Line Model (ALM) in the frame of Large Eddy Simulation method has been used to study different related topics, from wake stability to wind turbine interaction and wind farm control, and it is considered the state of the art to simulate with high fidelity the wind flow through wind turbines and wind farms. Despite that, the ALM results, particularly loads and power production, have shown to be dependent on the numerical setup, like the projection function and its smearing parameter. The present paper aims to contribute to the latter by showing the influence of limiting the projection region. It is found that projecting the aerodynamic forces onto a cylinder that confines the rotor disk improves the computed power and loads compared to a Blade Element Momentum code and affects the wake development.

1. Introduction

The Actuator Line Model (ALM) [1], combined with the Large Eddy Simulation method (LES) [2], has become the state of the art to simulate with a high fidelity approach the wind flow through wind turbines and wind farms. The ALM has been used to simulate stand alone wind turbines, cluster of wind turbines and wind farms, in some cases comparing the results with wind tunnel experimental campaigns as well as actual wind farms, see for instance [3–12]. For a review of the ALM and its application please see [13, 14].

In the ALM, as well as other actuator type models, the aerodynamic forces have to be projected onto the computational domain through a smearing function to smooth the applied forces in order to avoid the appearence of numerical oscillations [15]. In general, a Gaussian like 3D smearing function, characterized by one smearing parameter, is frequently used [15, 16]. One major drawback of the ALM is that the aerodynamic loads and hence the obtained power production depend on the smearing parameter, and larger power production is usually obtained when the smearing parameter is increased for the same numerical setup [6, 17]. Moreover, it has been shown that the aerodynamic loads are overpredicted close to the blade tip. Because of that,

work has focused on how to optimally project the aerodynamic forces looking for an optimal value of the smearing parameter. It has been recognized that, when using fine enough spatial resolution, the force distribution should resemble the pressure distribution along the span of the blade recovering the expected induced velocity [18–20]. Instead of looking for an optimal value of the smearing factor, in [21–23] it was argued that the main cause for the overprediction of aerodynamic loads near the tip are related to a missing induction generated by the formation of a viscous vortex core, originated from the 3D smearing of the forces. This viscous vortex core affects the bound and shed vorticity, changing the local wind speed and increasing the angle of attack. The results using the corrections presented in [21, 23] are improved compare with Blade Element Momentum method (BEM).

In [24] a set of guidelines are presented to setup a simulation with the ALM, including a recommended spatial resolution range. In order to reduce the computational cost those recommendations have to be relaxed. Recently, its use with coarse spatial resolution has been assessed by different authors [7, 9, 12, 17, 25, 26]. When using a coarse spatial resolution while simulating NREL 5MW reference wind turbine [27] in [23] the proposed correction reduces the peak difference with BEM from 77% to 17% for the tangential load. Based on the tangential load distribution the power production is still overpredicted.

Regarding the smearing function, as pointed out before, a 3D Gaussian kernel with one smearing factor is often used. There has been attempts to use a different approach, like in [28,29] where a 2D Gaussian kernel projecting the forces in the direction normal to each line or a 3D Gaussian kernel with 3 smearing factors are used respectively. In [28] it is stated that when using a 3D Gaussian smearing function the forces are spread beyond the limit of the actual tip. It should be stated that the proposed 2D Gaussian kernel still projects forces outside the rotor disk. Taking into account that the aerodynamic forces and local velocities at the lines representing the blades are interrelated, the former should not be distributed outside the rotor disk. If the aerodynamic forces are projected onto the numerical domain outside the rotor disk, a reduced force field is applied to the fluid particles that may pass through the rotor. As a consequence, the velocity at the lines representing the blades is larger, so the mass flow rate as well as the kinetic energy flux through the rotor disk are larger and the wind turbine will capture more power. This is particularly worst when using coarse spatial resolutions. In order to avoid this, in this work the aerodynamic forces are distributed using a 3D Gaussian function, consistent with the smearing correction presented in [30], limiting the projection region to a cylinder confined within the rotor disk.

The aim of the present paper is to evaluate the influence of the smearing correction and of the projection region on loads as well as power production of coarse LES-ALM simulations. To accomplish this, different cases are considered taking into account an atmospheric boundary layer inflow condition. In details, coarse LES-ALM simulations have been performed using nomerical models of both a multi-MW reference wind turbine [31] and of a state of the art wind tunnel experimental campaign [9] that makes use of identical G1 scaled models already used in previous research projects [32–34]. The focus of the simulations performed with the multi-MW wind turbine is to assess the load distribution along the blades and power, comparing results with BEM simulations, while the objective of the simulations performed with the scaled models is to evaluate the influence on power production as well as wake characteristics. The paper is organized as follows: Section 2 describes the numerical setups and experimental campaign considered, Section 3 presents the main results obtained and the conclusions are drawn in Section 4.

2. Methodology

LES-ALM simulations are performed with the open source finite volume code caffa3d [35, 36]. The ALM has been implemented in the code and used to simulate different cases, from

wind tunnel to actual wind farms, including wind turbine torque and pitch control actions [7–9, 12, 17, 29, 37–39].

In this paper two cases are considered: A) a multi-MW reference wind turbine (Section 2.1) and B) 3 model wind turbines (3 G1) placed in a wind tunnel (Section 2.2).

A brief description of the numerical domain is given in sections 2.1 and 2.2. For further details please see [9, 12].

Regarding the numerical setup for the LES-ALM simulations of both cases, a zero velocity gradient is imposed at the outlet and a wall model based on the log law is used to compute the stress at the surface while periodic conditions are used in the lateral boundaries. The Crank-Nicolson scheme is used to advance in time. The scale dependent dynamic Smagorinsky model with local averaging scheme is used to compute the subgrid scale stress. The convective term is approximated by an implicit term and an explicit deferred correction, combining a third order compact scheme with a fourth order central difference compact scheme [40]. The inflow conditions are obtained from precursor simulations, taking into account the same numerical setup but without wind turbine and applying a periodic boundary condition in the west and east boundaries and a constant pressure gradient as forcing term.

In both cases different setups have been tested: applying Prandtl tip loss correction factor (fP), applying the smearing correction proposed in [30] (SC), limiting the projection region to a cylinder confined within the rotor disk (Cyl).

A BEM code has been developed based on [41].

2.1. Multi-MW reference wind turbine

The reference wind turbine presented in [31] is used to compare LES-ALM simulations with BEM results. To accomplish that, a stand-alone wind turbine is simulated through LES-ALM. It is a variable speed, variable pitch wind turbine, with rated power, hub height and rotor diameter of 3.35MW, 110m and 130m respectively. The controller presented in [12] has been used for both the BEM and LES-ALM results.

The same domain as the one presented in [8, 12] is used. The size of the numerical domain is 3km x 1.5km x 0.75km in the streamwise, spanwise and vertical direction. The streamwise and spanwise directions are uniformly divided into 144 and 128 grid cells respectively, while a stretched grid is used in the vertical direction with 80 grid cells (23 grid cells cover a vertical diameter). This implies a spatial resolution (R1) of $R/3.125$ and $R/5.56$ in the streamwise and spanwise directions respectively (being R the rotor radius).

2.2. Wind tunnel case

The validation case is the one presented in [9], and consists of 3 model wind turbines G1, separated $4D$ in the streamwise direction and with a lateral shift of half a diameter and without yaw offset.

The same domain as the one presented in [9] is used. The size of the numerical domain is 27.5m x 5.5m x 4.5m in the streamwise, spanwise and vertical direction. The streamwise and spanwise directions are uniformly divided into 384 and 96 grid cells respectively, while a stretched grid is used in the vertical direction with 80 grid cells (29 grid cells cover a vertical diameter). This implies a spatial resolution of $R/7.68$ and $R/9.60$ in the streamwise and spanwise directions respectively.

3. Results

3.1. Multi-MW reference wind turbine

In this section the results of the simulations of the stand-alone reference wind turbine are presented. Figure 1 depicts the power production and RPM time histories obtained using a smearing parameter of 1.35 δx (E1), being δx the streamwise spatial resolution, and applying/not

applying Prandtl tip loss correction factor (fP) or the smearing correction proposed in [30] (SC) as well as the limitation in the projection region (Cyl). The best results compared to BEM are obtained when using the smearing correction (SC) including the projection region limitation (Cyl). The difference in mean power production compared to BEM is 20.7%, 0.3%, 37.1% and 13.7% for setups (SC), (SC+Cyl), (fP) and (fP+Cyl) respectively. The time lag seen in figure 1 between uBEM and LES-ALM is caused by the fact that the same inflow condition is used in both simulation approaches, but for the LES-ALM the inflow takes initially some time to reach the wind turbine rotor as it is placed two rotor diameters downstream from the inlet boundary. To get a deeper insight into the differences in power production obtained, the

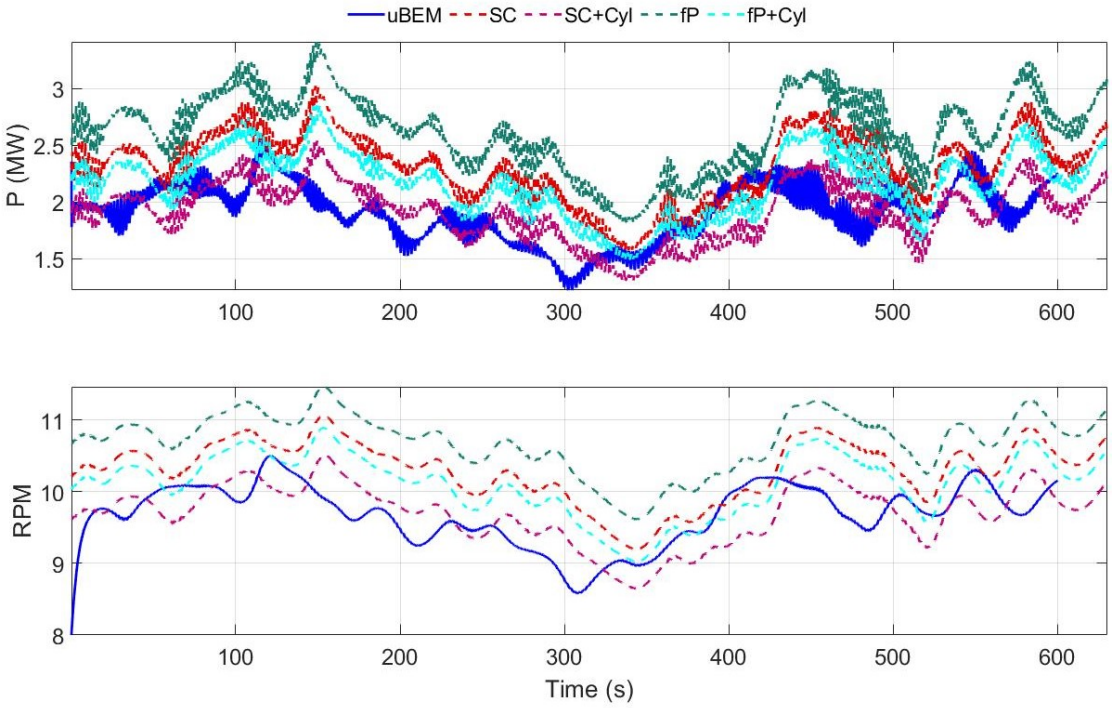

Figure 1. Power production (top) and RPM (bottom) time histories. uBEM power results are shifted in time due to the position of the wind turbine in the LES-ALM simulations. Case: multi-MW reference wind turbine. Smearing factor: E1.

normal and tangential mean loads are depicted in figure 2. As can be seen, better results of the mean loads are computed with the smearing correction (SC) rather than with Prandtl tip loss correction (fP). It should be mentioned that without limiting the projection region (Cyl) the smearing correction (SC) is able to get the desired behaviour of the force distributions but overpredicting its value for radius larger than $0.4R$. An excellent agreement with BEM is obtained with (SC+Cyl).

The variation in rotor speed observed in figure 1 (bottom) is the result of the wind turbine controller reaction to the different forces obtained by using the four projection methods discussed in this paper. However, the power and forces variation observed in figure 1 (top) and figure 2 are amplified by these rotor speed differences. Indeed, due to the different rotor speeds the tip speed ratio (TSR) at which the wind turbine operates also differs for the four proposed methods. As a consequence, the observed power variation is not only due to the different projection methods, but also to the different operating TSR. To only assess the influence of the proposed projecting methods, the same simulations setups are tested keeping the angular speed of the rotor at a fixed

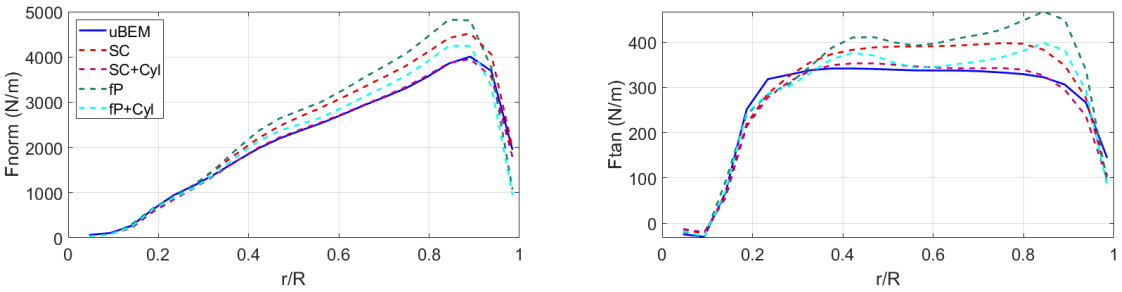

Figure 2. Mean normal and tangential loads along the blades (left and right respectively). Case: multi-MW reference wind turbine. Smearing factor: E1.

value, which thus allows to keep constant the operating TSR. Figure 3 depicts the normal and tangential mean loads along the blades and the time evolution of the power production. It can be observed that the best match with BEM results is obtained when using the smearing correction as well as the limitation in the projection region (SC+Cyl). The difference in mean power production compared to BEM is 16.6%, 0.2%, 28.0% and 11.7% for setups (SC), (SC+Cyl), (fP) and (fP+Cyl) respectively. As expected, such results indicate that the effects on forces, and therefore power, of the four projection methods discussed in this paper are less significant when the TSR is kept constant. In the following of this paper, however, the reported results will regard the ouputs of simulations obtained by letting the wind turbine controller defining the wind turbine rotating speed.

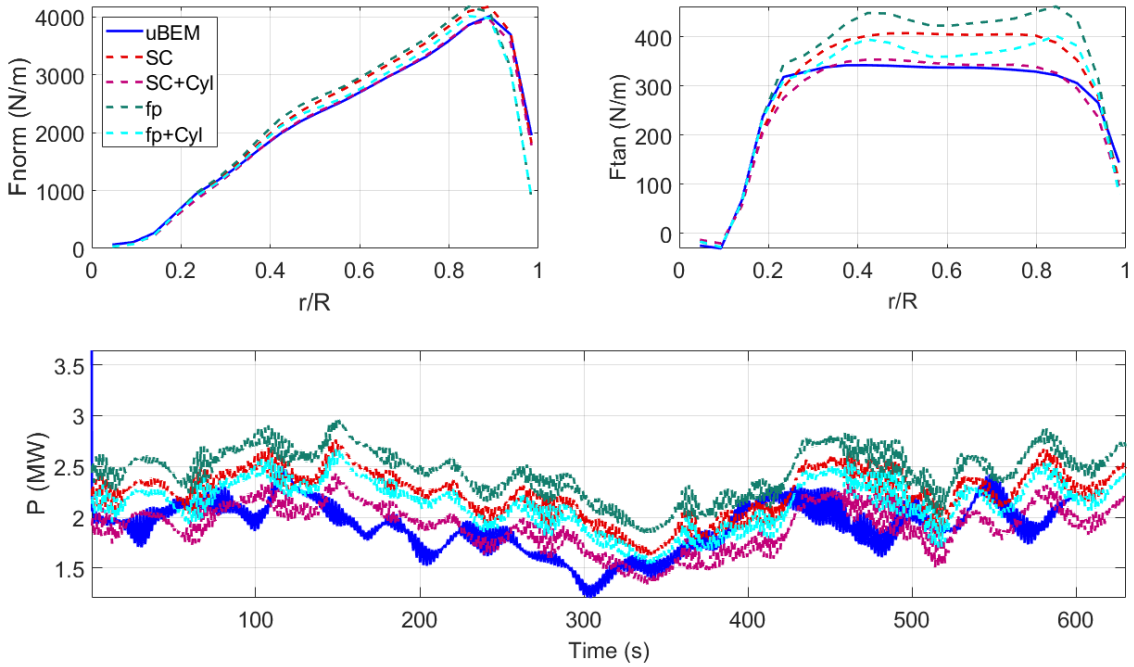

Figure 3. Mean normal and tangential loads along the blades (top: left and right respectively) and power production (bottom). RPM: fixed. Case: multi-MW reference wind turbine. Smearing factor: E1.

When looking at the mean streamwise velocity component at a vertical plane passing through the rotor plane presented in figure 4, it is clear that applying the limitation in the projection region (Cyl) lowers the wind speed at the disk as larger forces are applied in front of the rotor disk. In this way, two mechanisms are playing together: on one hand the forces are projected onto the numerical domain affecting the expected flow region and on the other hand as the forces are spread over a smaller region its value in each cell is larger. As a result, the aerodynamic loads are lower and the wind turbine operates at a lower angular velocity and produces less power as shown above.

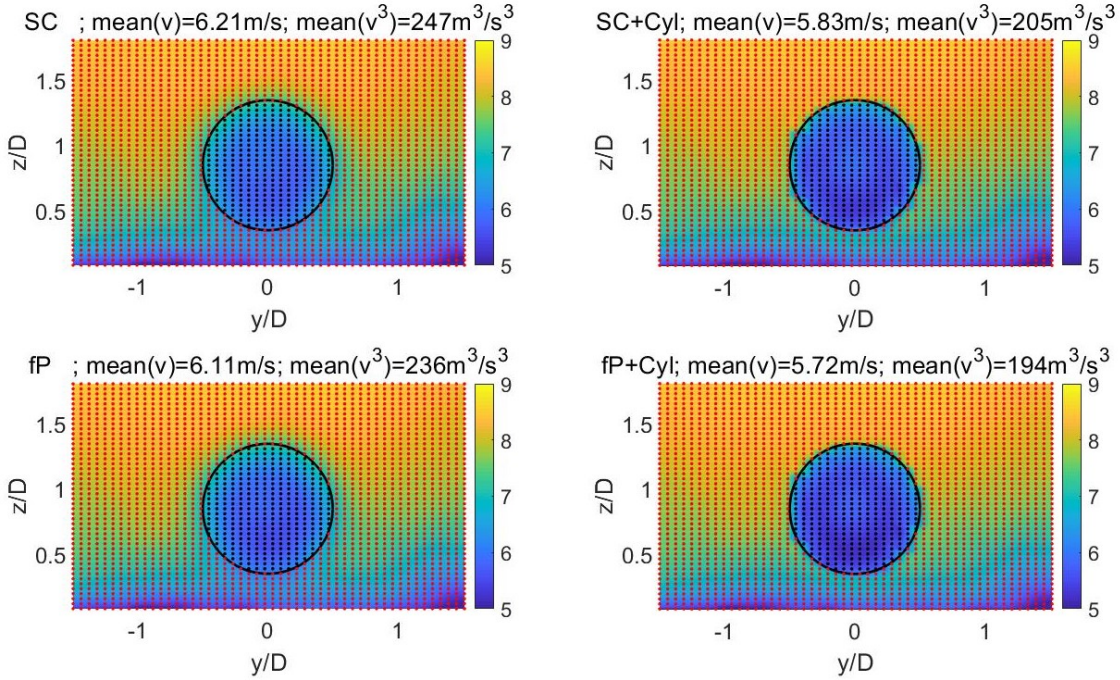

Figure 4. Mean streamwise velocity component at a vertical plane passing through the rotor plane. Black and red dots: points with interpolated data from the CFD grid outisde and inside the rotor disk, respectively. The title of each subplot includes the mean streamwise velocity component and the mean value of the kinetic energy flux per unit mass. Case: multi-MW reference wind turbine. Smearing factor: E1.

Regarding the wake, figures 5 and 6 present the mean streamwise velocity component (U) and turbulence intensity (TI), respectively, at different locations in the wake at hub height. There are almost no differences between applying the smearing correction (SC) or Prandtl tip loss correction (fP) in U, however applying the restriction in the projection region (Cyl) greatly influences the results between $5D$ and $10D$. A different trend is observed in the TI profiles, as the main differences are in the near wake ($< 4D$), where larger peaks of TI are obtained when limiting the projection region. The larger TI explains the faster wake recovery seen.

To assess the influence of the smearing factor and spatial resolution in the above results, further simulations were performed. First, simulations with the same numerical setup but using a smearing factor of 2.00 δx (E2, +48% larger than E1) are presented.

Figure 7 depicts the normal and tangential mean loads along the span of one blade when applying or not the projection region restriction and the smearing correction (SC) or Prandtl tip loss correction (fP) while setting the smearing factor at a value of E1 or E2. The electric power has been presented in the figure instead of the aerodynamic power to simplify the

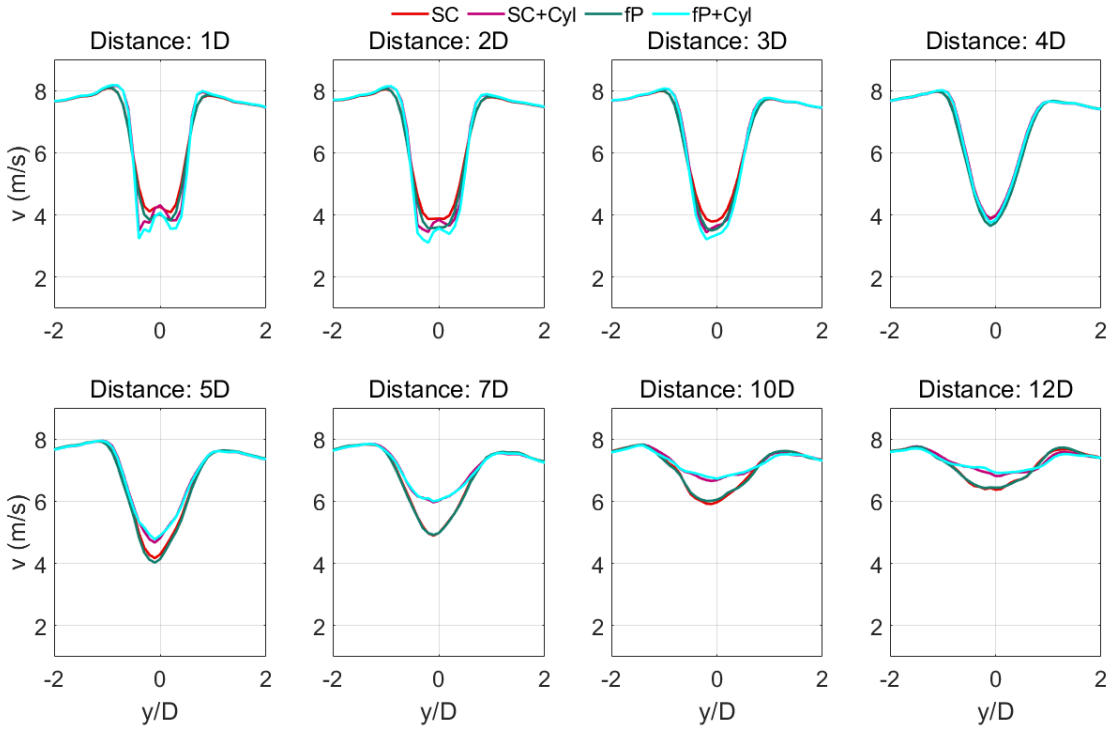

Figure 5. Mean streamwise velocity component at different locations in the wake at hub height. Case: multi-MW reference wind turbine. Smearing factor: E1.

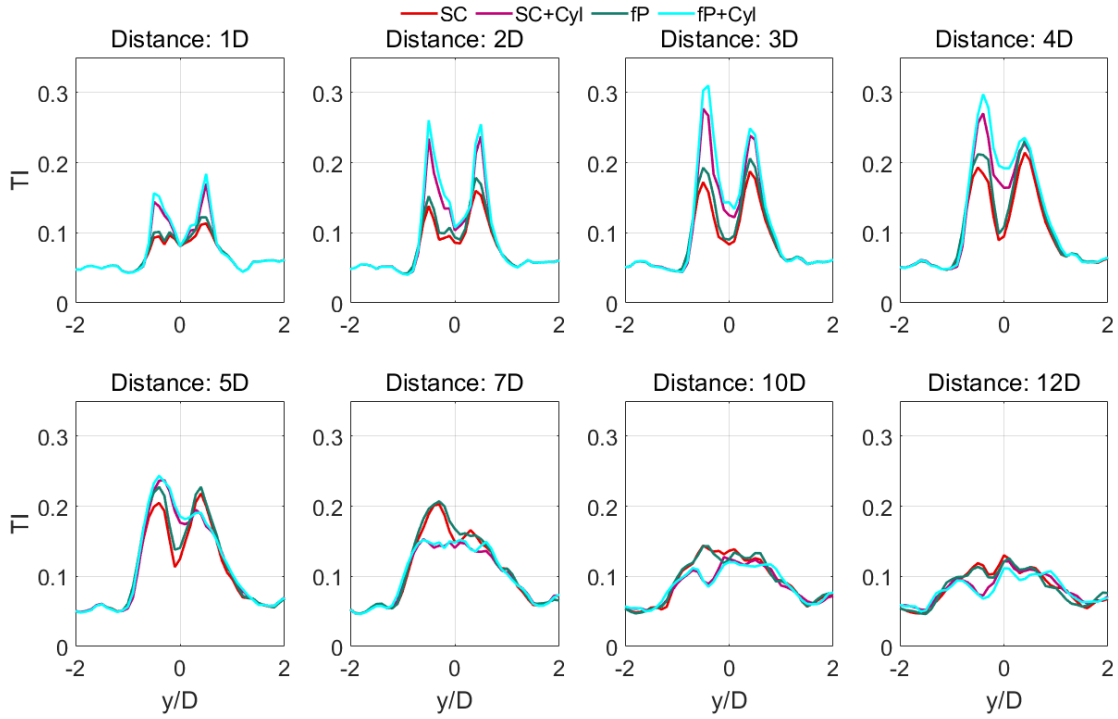

Figure 6. Turbulence intensity at different locations in the wake at hub height. Case: multi-MW reference wind turbine. Smearing factor: E1.

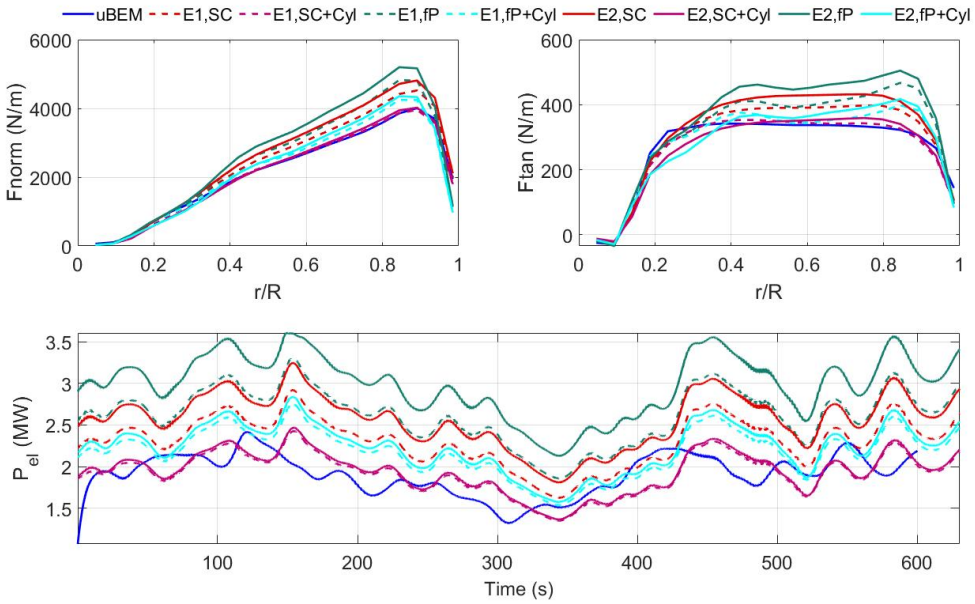

Figure 7. Mean normal and tangential loads along the blades (top, left and right respectively) and electric power time history (bottom). Case: multi-MW reference wind turbine.

comparison. From the figure it can be observed that both loads and electric power are well captured by applying the smearing correction (SC) with the limitation in the projection region (Cyl) independently of the value of the smearing parameter. The mean power computed using E1 and E2 deviates from the BEM results by 0.3% and 1.7% respectively. It should be mentioned that these values increase to 20.7% and 34.3% when using the smearing correction (SC) without limiting the projection region. From the above it can be concluded that when changing the smearing factor from E1 to E2 and applying the smearing correction (SC) without the limitation in the projection region the power increases 11.3% while when including the restriction in the projection region the power increases 1.3%. Regarding the wake, a similar observation as before can be drawn from the mean streamwise velocity component (U) and turbulence intensity (TI) profiles, the main difference is driven by applying or not the restriction of the projection region: U profiles are quite similar for the numerical setups where the limitation in the projection region is applied (is not applied) at distances larger than $4D$. A similar observation, for the case without the projection region restriction, is made in [42].

To assess the influence of the spatial resolution, LES-ALM simulations with the smearing correction (SC) and with/without the projection region limitation (Cyl) are performed taking into account the same domain uniformly divided into 192 x 144 grid cells in the streamwise and spanwise directions, $R/4.17$ and $R/6.2$, respectively, while 96 grid cells are used in the vertical direction (29 grid cells cover a vertical diameter) (R0, [8]). The same numerical setup, but with a new precursor simulation, is used. Figure 8 depicts the normal and tangential mean loads of the LES-ALM simulations and the BEM results, normalized by $1/2\rho AU$ (being U the mean streamwise velocity component at a horizontal plane close to the inlet and A the rotor sweep area). From the figure it can be observed that a better agreement with BEM is obtained when using the limitation in the projection region (Cyl). The difference in mean power computed is +11.2% and -0.5% for setups SC and SC+Cyl respectively.

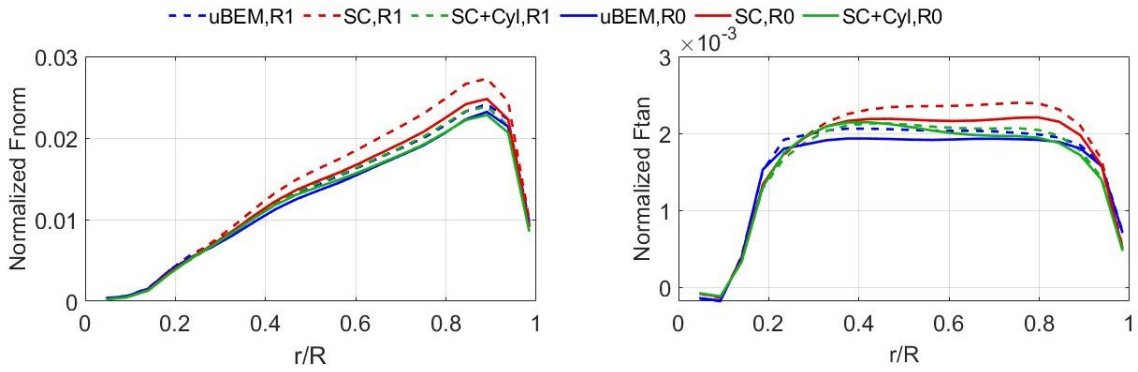

Figure 8. Mean normalized loads along the blades (left: normal force, rigth: tangential force). Case: multi-MW reference wind turbine. Spatial resolution: R1 and R0.

3.2. Wind tunnel case

In the previous section the influence of different numerical setups related to the computation of the aerodynamic loads particularly close to the tip and their projection onto the computational domain is assessed. From the above it is observed that the wake characteristics are affected by those changes. To get an insight into the influence of the setup on the wake, a different validation case has been simulated in order to compare the numerical results with wind tunnel data.

The mean power production and RPM are presented in figure 9 (WTG1 is the furthest upstream wind turbine, followed by WTG2 and WTG3). Looking at the second and third wind turbines the best agreement between the experimental data and the numerical results is obtained when applying the smearing correction (SC) and limiting the projection region (Cyl). The results of the first wind turbine in the row are not consistent. In the figure the mean value obtained with the BEM code is included. The better agreement between BEM and LES-ALM simulations is again when using that setup (SC+Cyl). The difference between LES-ALM results and BEM compared to the experimental data may be related to the fact that the inflow generated by the wind tunnel is not homogeneous in the spanwise direction, with variations in flow velocity up to 6% [43].

Figure 10 shows the mean streamwise velocity component 0.10m above hub height at different locations in the wake for the same setups, including the experimental data. It can be seen that the simulated results are in quite good agreement with the experimental data and that there is no big difference between the setups tested for the locations considered. These results are consistent with the ones obtained before. As the wind turbine models are separated $4D$ in the streamwise direction, it is not possible to analyze the influence of the numerical setups further downstream in the wake as shown above. In the near future the authors will simulate other validation cases, particularly with wake measurements in the far wake and wind turbines separated more than $4D$ in the streamwise direction.

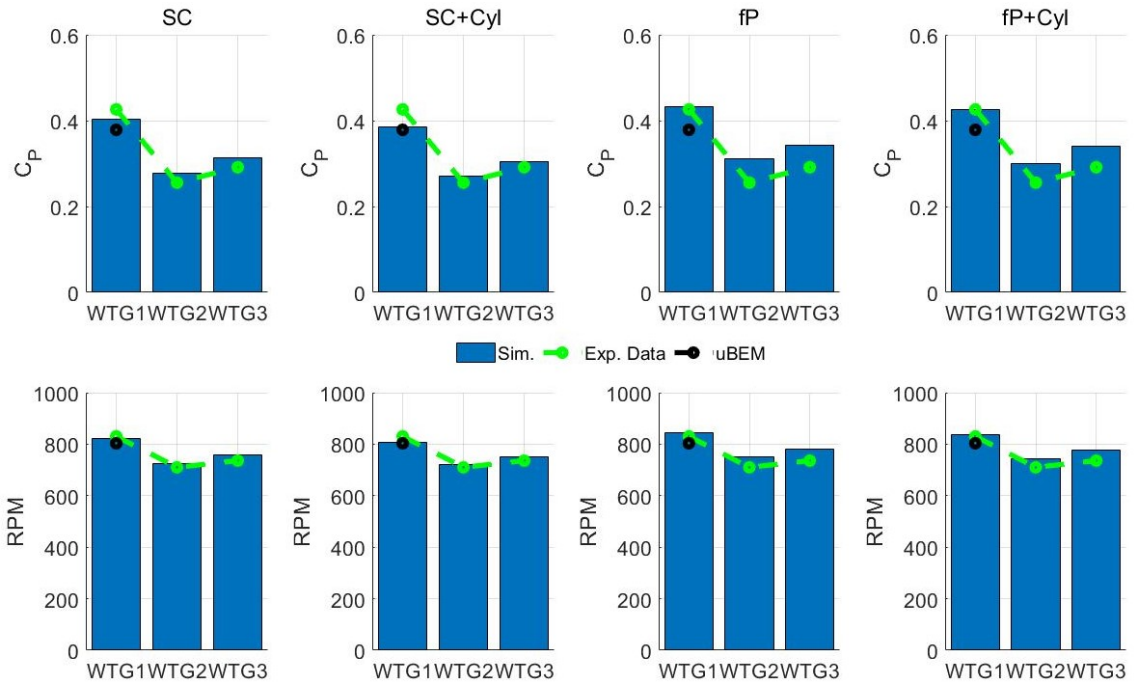

Figure 9. Mean power production (top) and angular velocity (bottom). Case: 3 G1.

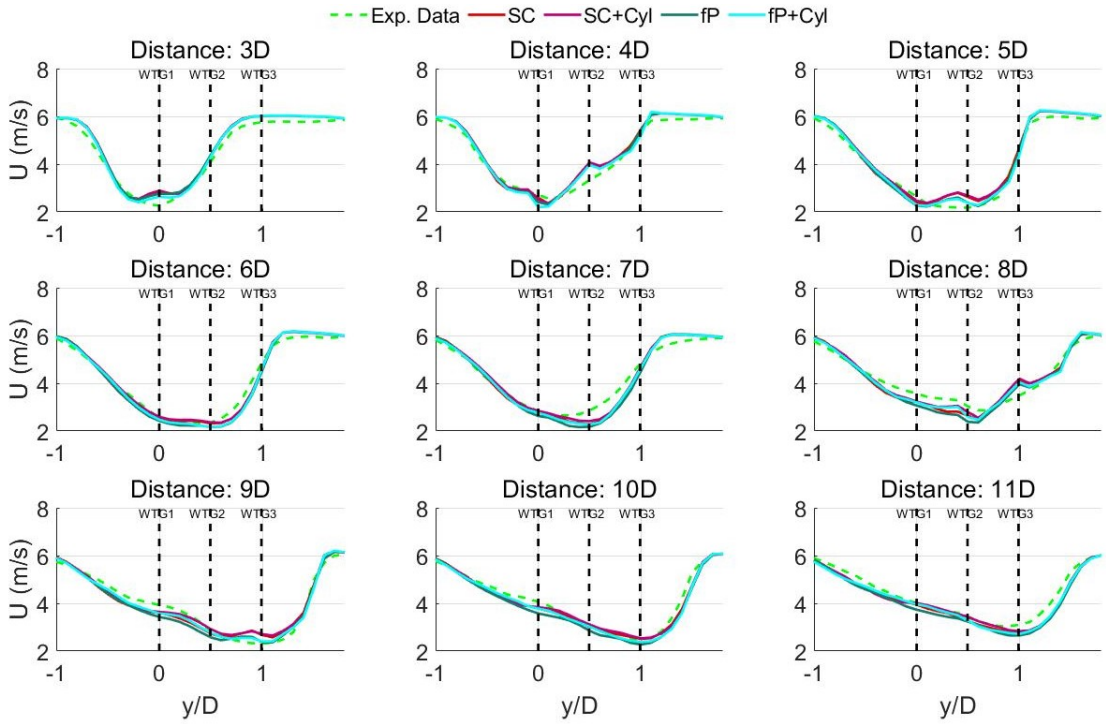

Figure 10. Mean streamwise velocity component at different locations in the wake. Distance measured from the rotor plane of WTG1, being D the rotor diameter. Case: 3 G1.

4. Conclusions

The Actuator Line Model has become the state of the art to simulate with high fidelity the wind flow through wind turbines and wind farms. The computed loads and power have shown to be dependent on the numerical setup, particulary the smearing parameter related to the projection function. Recently new corrections have been proposed aiming to compute the missed induction generated by the smearing of the forces, aiming to get the expected load distribution.

In this paper Large Eddy Simulation-Actuator Line Model simulations (LES-ALM), using coarse spatial resolutions, have been performed in order to assess the influence of different setups concerning the tip treatment and the projection function used, looking for improving the loads and power estimations, limiting the projection region in order to affect the expected flow region in front of the rotor disk. Different simulation cases have been considered, comparing the results with Blade Element Momentum (BEM) computations and experimental data when available. The main conclusion and contribution of this work is that applying the aerodynamic forces onto the computational domain in the adequate region, a cylinder confining the rotor disk, plays a major role in LES-ALM simulations.

References

[1] Sørensen J N and Shen W Z 2002 *Journal of fluids engineering* **124** 393–399
[2] Sagaut P 2006 (Springer Science & Business Media)
[3] Churchfield M, Lee S, Moriarty P, Martinez L, Leonardi S, Vijayakumar G and Brasseur J 2012 *50th AIAA Aerospace Sciences Meeting including the New Horizons Forum and Aerospace Exposition*
[4] Porté-Agel F, Wu Y T, Lu H and Conzemius R J 2011 *Journal of Wind Engineering and Industrial Aerodynamics* **99** 154–168 ISSN 01676105
[5] Xie S and Archer C 2015 *Wind Energy* **18** 1815–1838
[6] Martínez-Tossas L A, Churchfield M J and Leonardi S 2015 *Wind Energy* **18** 1047–1060
[7] Draper M, Guggeri A and Usera G 2016 *Journal of Physics: Conference Series* vol 753 (IOP Publishing) p 082007
[8] Guggeri A, Draper M and Usera G 2017 *Journal of Physics: Conference Series* vol 854 (IOP Publishing) p 012018
[9] Draper M, Guggeri A, Mendina M, Usera G and Campagnolo F 2018 *Journal of Wind Engineering and Industrial Aerodynamics* **182** 146–159
[10] Deskos G and Piggott M D 2018 *Wind Energy* **21** 1266–1281
[11] Yang X, Pakula M and Sotiropoulos F 2018 *Applied Energy* **229** 767–777 ISSN 0306-2619
[12] Guggeri A and Draper M 2019 *Energies* **12** 3508
[13] Sørensen J N, Mikkelsen R F, Henningson D S, Ivanell S, Sarmast S and Andersen S J 2015 *Philosophical Transactions of the Royal Society A: Mathematical, Physical and Engineering Sciences* **373** 20140071
[14] Breton S P, Sumner J, Sørensen J N, Hansen K S, Sarmast S and Ivanell S 2017 *Philosophical Transactions of the Royal Society A: Mathematical, Physical and Engineering Sciences* **375** 20160097
[15] Troldborg N 2008 Ph.D. thesis Technical University of Denmark
[16] Ivanell S 2009 Ph.D. thesis KTH Royal Institute of Technology
[17] Draper M and Usera G 2015 *Journal of Physics: Conference Series* vol 625 (IOP Publishing) p 012021
[18] Shives M and Crawford C 2013 *Wind Energy* **16** 1183–1196
[19] Martínez-Tossas L A, Churchfield M J and Meneveau C 2016 *Journal of Physics: Conference Series* vol 753 (IOP Publishing) p 082014
[20] Martínez-Tossas L A, Churchfield M J and Meneveau C 2017 *Wind Energy* **20** 1083–1096
[21] Forsting A M, Pirrung G and García N R 2019 *Wind Energy Science* **4** 369–383
[22] Dağ K O 2017 Ph.D. thesis Technical University of Denmark
[23] Dağ K O and Sørensen J N 2020 *Wind Energy* **23** 148–160
[24] Jha P K, Churchfield M J, Moriarty P J and Schmitz S 2014 *Journal of Solar Energy Engineering* **136** 031003
[25] Martinez L A, Meneveau C and Stevens R 2016 *34th Wind Energy Symposium* p 1261
[26] Stevens R J, Martínez-Tossas L A and Meneveau C 2018 *Renewable energy* **116** 470–478
[27] Jonkman J, Butterfield S, Musial W and Scott G 2009 Tech. rep. National Renewable Energy Lab.(NREL), Golden, CO (United States)
[28] Mikkelsen R 2003 Ph.D. thesis Technical University of Denmark

[29] Draper M, Guggeri A and Usera G 2016 *Journal of Physics: Conference Series* vol 753 (IOP Publishing) p 082028
[30] Meyer Forsting A R, Pirrung G and Ramos-García N 2020 *Wind Energy Science* **5** 349–353
[31] Bortolotti P, Tarres H C, Dykes K L, Merz K, Sethuraman L, Verelst D and Zahle F 2019 Tech. rep. National Renewable Energy Lab.(NREL), Golden, CO (United States)
[32] Campagnolo F, Petrović V, Bottasso C L and Croce A 2016 *Proceedings of the American Control Conference (ACC)* 513–518
[33] Campagnolo F, Petrović V, Nanos E M, Tan C W, Bottasso C L, Paek I, Kim H and Kim K 2016 *Proceedings of the The 26th International Ocean and Polar Engineering Conference* (Rhodes, Greece)
[34] Wang J, Bottasso C and Campagnolo F 2016 *Journal of Physics: Conference Series* vol 753 (IOP Publishing) p 032064
[35] Usera G, Vernet A and Ferré J A 2008 *Flow, Turbulence and Combustion* **81** 471–495
[36] Mendina M, Draper M, Soares A P K, Narancio G and Usera G 2013 *Cluster Computing* **17** 231–241
[37] Draper M, Guggeri A, López B, Díaz A, Campagnolo F and Usera G 2018 *Journal of Physics: Conference Series* vol 1037 (IOP Publishing) p 072051
[38] Guggeri A, Draper M, López B and Usera G 2019 *Journal of Physics: Conference Series* vol 1256 (IOP Publishing) p 012030
[39] Mühle F, Schottler J, Bartl J, Futrzynski R, Evans S, Bernini L, Schito P, Draper M, Guggeri A, Kleusberg E *et al.* 2018 *Wind Energy Science* **3** 883–903
[40] Ferziger J H and Peric M 2002 3rd ed (Springer-Verlag Berlin Heidelberg)
[41] Hansen M O 2015 (Routledge)
[42] Forsting A R M, Pirrung G R and Ramos-García N 2019 *Journal of Physics: Conference Series* vol 1256 (IOP Publishing) p 012020
[43] Wang J, Foley S, Nanos E, Yu T, Campagnolo F, Bottasso C L, Zanotti A and Croce A 2017 *Journal of Physics: Conference Series* vol 854 (IOP Publishing) p 012048